Available online at www.sciencedirect.com
SCIENCE DIRECT®
Journal of Molecular Catalysis A: Chemical 216 (2004) 233–245
JOURNAL OF MOLECULAR CATALYSIS A: CHEMICAL
www.elsevier.com/locate/molcata

Pt thin films on stepped $SrTiO_3$ surfaces: $SrTiO_3$(6 2 0) and $SrTiO_3$(6 2 2)

Aravind Asthagiri[1], David S. Sholl*

Department of Chemical Engineering, Carnegie Mellon University, Pittsburgh, PA 15213, USA

Available online 27 April 2004

Abstract

As a first step in understanding Pt growth on chiral $SrTiO_3$ surfaces we have examined Pt adsorption on the stepped $SrTiO_3$(6 2 0) and $SrTiO_3$(6 2 2) surfaces using plane-wave density functional theory. We find that for both stepped $SrTiO_3$ surfaces Pt adsorbs more strongly along the step versus the terrace. We also report on the interface strength of Pt slabs on both terminations of $SrTiO_3$(6 2 0) and (6 2 2). We find that the interface strength is considerably larger than found for Pt slabs on the low-Miller index $SrTiO_3$ surfaces. Our results indicate that step-flow growth of Pt that retains the underlying morphology of the stepped $SrTiO_3$ surface is likely to be favored over island nucleation on terraces. This preliminary work indicates that the growth of thin metal films on chiral metal oxides may be a viable approach to producing cheap chiral metal surfaces.

Keywords: Low-Miller index; Pt slab; Chiral metal surface

1. Introduction

There has been considerable recent interest in naturally chiral metal surfaces [1–4]. These chiral surfaces can be obtained by cutting a metal crystal along a high-Miller index plane, yielding terraces separated by monoatomic kinked steps [5,6]. For a thorough discussion of chiral surfaces and a review of recent experimental and theoretical work, see [1,4]. It has been shown both experimentally and theoretically that chiral metal surfaces can differentiate between adsorbed enantiomers and the resulting energy differences can be on the same order as those exploited in current chiral chromatography techniques [1,7]. Of course, for effective separations or catalysis large surface areas are required, strongly limiting the feasibility of single-crystal chiral metal surfaces in practical situations. One potential route around this difficulty is to epitaxially grow metal overlayers on a chiral metal oxide surface. There are hundreds of metal oxides that can be chiral due to their bulk structure [1,8] or can reveal chiral surfaces if cut along appropriate planes. Furthermore crystalline metal oxides can be found that are substantially cheaper than catalytic metals. If metal films can be deposited on a chiral metal oxide while retaining the atomic geometry of the underlying substrate, this could be a feasible method to obtain practical quantities of chiral metal surfaces.

To seek a proof of principle for the idea described above, we have worked with our experimental collaborators at Carnegie Mellon University to understand and control the epitaxial growth of Pt on $SrTiO_3$ surfaces [9–11]. The structure of bulk $SrTiO_3$, a cubic perovskite material, is shown in Fig. 1. $SrTiO_3$ has been widely used as a substrate for growth of other oxides, including layered high-T_c superconductors [12–14]. The bulk lattice constants of Pt and $SrTiO_3$ are very similar; 3.923 and 3.905 Å, respectively, at room temperature [15,16]. This fact, combined with the low oxygen affinity of Pt, suggests that epitaxial films of Pt may be grown on $SrTiO_3$ substrates [15,16]. Miller Index surfaces of $SrTiO_3$ have two possible surface terminations. The ideal truncation of bulk $SrTiO_3$ along the (1 0 0) plane results in a structure with alternating SrO and TiO_2 layers, as shown in Fig. 1(a). Therefore, $SrTiO_3$(1 0 0) can have either a SrO-terminated or a TiO_2-terminated surface. Similarly, the ideal truncation of $SrTiO_3$(1 1 1) has either a SrO_3-terminated or a Ti-terminated surface, as shown in Fig. 1(b). $SrTiO_3$(1 1 1) is termed a polar surface because the ideal layers along the surface normal have a nonzero

* Corresponding author. Tel.: +1-412-268-4207; fax: +1-412-268-7139.
E-mail address: sholl@andrew.cmu.edu (D.S. Sholl).
[1] Present address: Geophysical Laboratory, Carnegie Institution of Washington, Washington, DC 20015, USA.

1381-1169/$ – see front matter © 2004 Elsevier B.V. All rights reserved.
doi:10.1016/j.molcata.2004.03.011

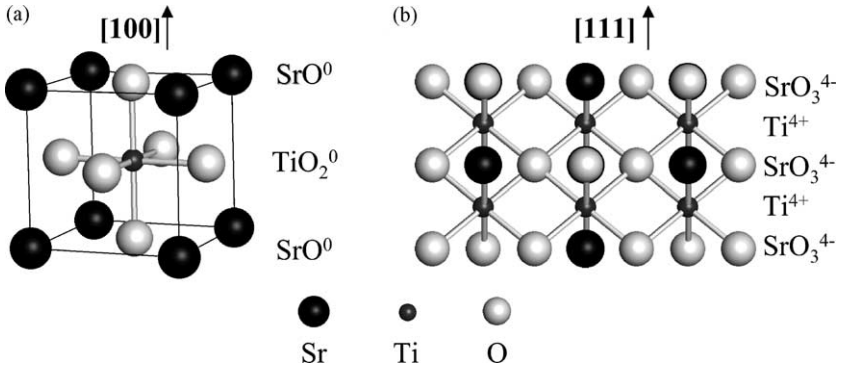

Fig. 1. Structural representations of $SrTiO_3$. The (1 0 0) direction is highlighted in (a), while (b) shows a side view of the SrO_3-terminated (1 1 1) surface.

net charge, which results in a net dipole for the repeat unit. A thorough discussion of polar oxide surfaces including a survey of both experimental and theoretical studies of these systems is given in [17].

Chiral $SrTiO_3$ surfaces can be obtained in the same manner as Pt chiral surfaces by cutting along a high-Miller index plane [1]. A picture of the ideally terminated $SrTiO_3$(6 4 3) surface is shown in Fig. 2. This chiral surface has (1 1 1) terraces and the long and short steps are (1 0 0) and (1 1 0) microfacets, respectively, completely analogous to the fcc(6 4 3) structure that has been widely studied in previous work on naturally chiral metal surfaces [1–4]. Unlike metal surfaces, the chemical composition of the steps and terraces vary on chiral $SrTiO_3$ surfaces, as can be seen by examining the long steps found in the unit cell. For each step in Fig. 2, the long step alternates between O–O–O and Sr–O–Sr chains. Similar observations can be made for the (1 1 0) step and the terrace. This results in a unit cell that is four times as large as the equivalent Pt(6 4 3) surface. The situation is further complicated by noting that we have shown only one of the possible terminations for $SrTiO_3$(6 4 3). Real $SrTiO_3$(6 4 3) surfaces will in general have a distribution of both terminations. It may be possible with the proper sample preparation method to control the surface termination, but these methods are not trivial to develop [10].

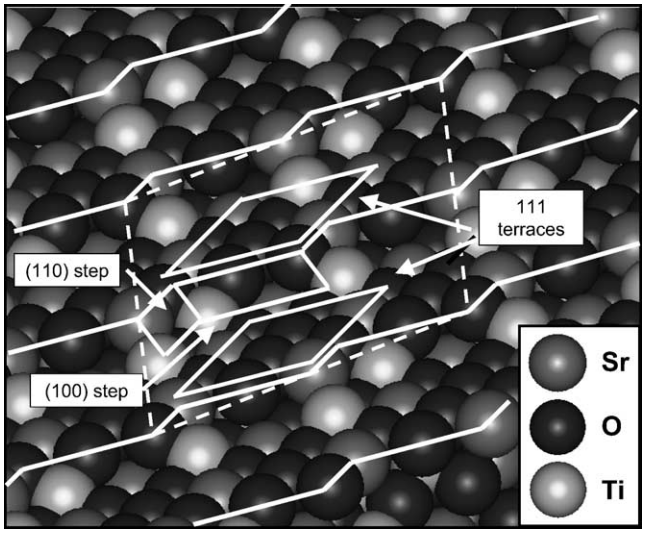

Fig. 2. Ball model of the chiral $SrTiO_3$(6 4 3) surface. Step edges and the microfacets making up the surface are indicated by solid lines and the unit cell is shown by the dashed box. The key for the atoms is shown in the inset and is used in the rest of the figures in the paper.

The discussion above has concentrated on a single chiral $SrTiO_3$ surface, $SrTiO_3$(6 4 3). There are, of course, a myriad of candidate chiral $SrTiO_3$ surfaces for Pt thin film growth. This raises several interesting questions. Are there certain surfaces that are preferable for growing chiral Pt films? What impact does the termination have on the growth process? Is it worth pursuing an experimental procedure to control the termination? Ideally we would like to use theoretical calculations to answer these questions and develop guiding principles to assist experimental work on this topic. To do this we have used plane-wave density functional theory (DFT) to evaluate the energetics of Pt on various $SrTiO_3$ surfaces. The use of DFT provides an important complement to the ongoing experimental studies of Pt/$SrTiO_3$ interfaces, providing, for example, direct information about the interface strength and structure that is difficult to obtain experimentally.

Examining a chiral surface like $SrTiO_3$(6 4 3) using DFT is computationally expensive because of the size and complexity of the system. We have taken the approach of starting our examination from the simplest surfaces, namely the achiral low-Miller index $SrTiO_3$ surfaces, and then based on these calculations proceed to surfaces with steps and kinks. We have already performed extensive calculations of Pt on all three low-Miller index surfaces of $SrTiO_3$ and these have been reported elsewhere [9,10,18]. While the low-Miller index surfaces are not chiral, microfacets of low-Miller index surfaces are the building blocks for chiral surfaces [1]. The next logical stage for our work is to examine the behavior of Pt near step edges on $SrTiO_3$ substrates.

Two relevant questions at this stage are: (1) what type of information can we obtain from applying DFT to Pt on stepped $SrTiO_3$ surfaces? and (2) is there an order of importance to the stepped surfaces we could possibly examine? Our previous work on low-Miller index $SrTiO_3$ surfaces

strongly suggested that the interface strength of Pt films is directly linked to the likelihood of achieving epitaxial growth experimentally. For stepped $SrTiO_3$ surfaces, our goal is to achieve epitaxial growth that retains the step structure. In studies of metal homoepitaxy, when growth occurs from the step bottoms out to the terrace the resulting morphology is frequently smooth and retains the step structure of the substrate [19]. This type of growth is termed step-flow growth. Step-flow growth is possible when adatoms do not nucleate to form islands on the terrace and instead attach to steps. There are many factors that determine if step-flow growth actually occurs including the deposition rate, the terrace width, and adatom diffusion kinetics. We cannot completely probe all these factors using DFT. We will concentrate on examining Pt adsorption sites on stepped substrates with the aim of determining if Pt adatoms prefers to adsorb along the step edge rather than on the terrace. To our knowledge there has been only one other DFT study of metal adsorption on stepped metal oxides [20]. This study examined Pd adatoms and clusters on stepped α-$Al_2O_3(0\,0\,0\,1)$ surfaces and found that the steps bound the Pd atoms more strongly than the terrace, an observation corroborated by STM experiments [21].

It is well known that metal oxide surfaces can be affected by reconstructions or the appearance of defects such as O vacancies. For instance, $SrTiO_3(1\,0\,0)$ can reconstruct into (2×1), (4×2), and (6×2) forms as a function of O_2 partial pressure and annealing temperature [22]. It is a nontrivial task to identify the conditions for a particular reconstruction and then characterize the detailed structure. Recently Erdman et al. were able to deduce the detailed structure of the (2×1) $SrTiO_3(1\,0\,0)$ reconstruction using a combination of high-resolution electron microscopy and DFT calculations [22]. While low-Miller index $SrTiO_3$ surfaces have been examined experimentally, we know of no experimental work on $SrTiO_3$ with high step densities. Therefore we are limited in our knowledge of the true structure of the stepped $SrTiO_3$ surfaces discussed in this paper. Several groups have included the effects of the environment and temperature using DFT to make thermodynamic-based predictions of the expected surface structure of metal oxides [23–25], but these calculations are extremely intensive and require a set of informed guesses of possible surface structures from experimental data. For our purposes, starting with the ideal stepped structures is a logical first step until future experimental work can provide definite indications of more complex structures that exist for real surfaces.

The step structures we have chosen to examine are the ideal terminations of $SrTiO_3(6\,2\,0)$ and $SrTiO_3(6\,2\,2)$. These stepped $SrTiO_3$ surfaces are shown in Fig. 3(a) and (b) and consist of terraces of $(1\,0\,0)$ orientation with $\{1\,1\,0\}$ and $\{1\,1\,1\}$ steps, respectively. The structure of these surfaces is discussed in more detail below. Unreconstructed $SrTiO_3(1\,0\,0)$ surfaces can be obtained experimentally [16], although it is not known if this extends to close packed stepped $SrTiO_3$ structures vicinal to $(1\,0\,0)$. We stress that $SrTiO_3(6\,2\,0)$ and $SrTiO_3(6\,2\,2)$ are achiral, but chiral $SrTiO_3$ surfaces vicinal to $(1\,0\,0)$ are composed of combinations of these two types of steps. One such combination is illustrated in Fig. 3(c), where the $SrTiO_3(6\,2\,1)$ surface

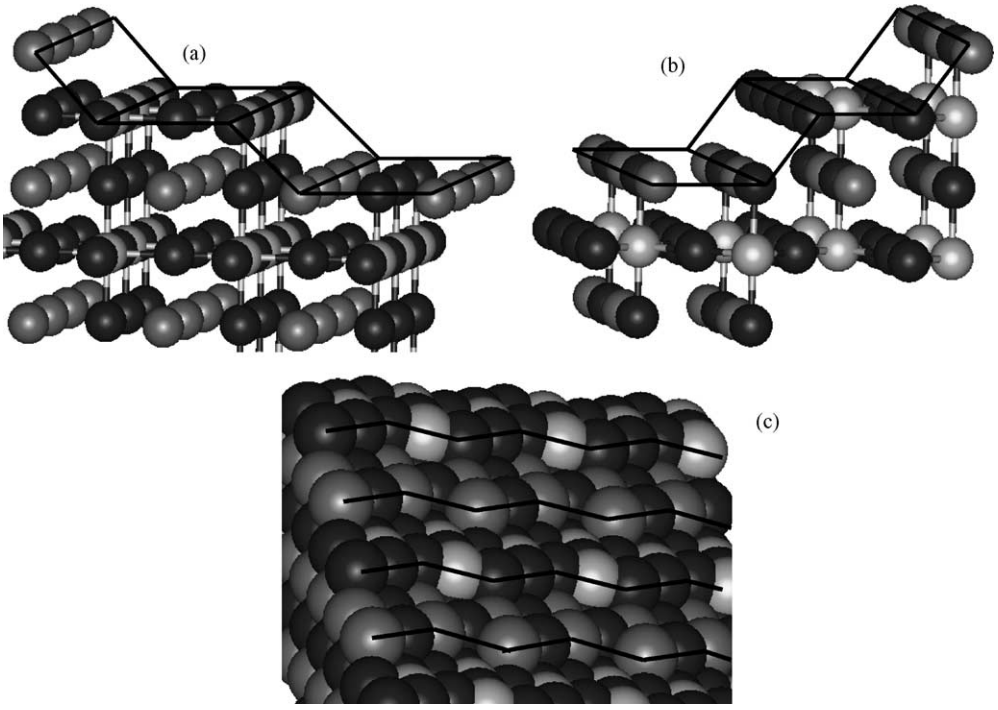

Fig. 3. Ball model of (a) $SrTiO_3(6\,2\,0)$, (b) $SrTiO_3(6\,2\,2)$ and (c) $SrTiO_3(6\,2\,1)$. All three surfaces are vicinal to $(1\,0\,0)$. Only one of the two distinct terminations for each surface is shown. Dark lines indicate step and terrace edges in (a) and (b), while the dark lines in (c) indicate step edges.

is shown. Our choice of these two surfaces is based on our earlier work on the low-Miller index surfaces. From this work, we know that Pt on nonpolar $SrTiO_3$(1 0 0) has a much weaker interface than Pt on the two polar low-Miller index surfaces [9,10,18]. As noted earlier, the probability of attaining step-flow growth is enhanced, when the deposited atoms have a stronger preference for the step edges than the terraces. Based on this logic we choose to focus on stepped surfaces vicinal to (1 0 0) since the terraces on these surfaces should have weaker interactions with Pt than surfaces vicinal to (1 1 0) or (1 1 1).

The rest of the paper is organized as follows. Section 2 discusses the DFT calculation details for the stepped $SrTiO_3$ surfaces. Sections 3 and 4 discuss our DFT results for $SrTiO_3$(6 2 0) and $SrTiO_3$(6 2 2), respectively. We have examined several potential Pt adsorption sites on both surfaces along with the interface strength of Pt slabs adsorbed on both surfaces. In Section 5 we will discuss the implications of these calculations for Pt growth on $SrTiO_3$ surfaces vicinal to (1 0 0). We conclude by discussing potential near and long term future work to shed more light on Pt growth on chiral $SrTiO_3$ surfaces.

2. Calculation details

All the DFT calculations in this paper were performed using VASP (Vienna ab initio simulation package) [26–29] with the ion cores represented by the norm-conserving ultrasoft-pseudopotentials found in the database provided by VASP [30–33]. The details outlined below have been used for all calculations in this paper and are very similar to the conditions of our earlier work on Pt adsorption on the low-Miller $SrTiO_3$ surfaces [9,10]. For Sr and Ti atoms the 4p and 3p orbitals, respectively, were included as valence states. Calculations have been done using the LDA (CA) [34] approximation for the exchange potential. We have done extensive GGA calculations in our previous work on low-Miller index $SrTiO_3$ surfaces and found that while there are quantitative differences between results from the two functionals, both methods yield the same qualitative trends [9,10,18]. This is similar to the finding of several other DFT studies of metal/metal oxide systems [35,36]. A plane-wave expansion with a cutoff of 340 eV was used for all calculations. Total energy calculations are done using the conjugate-gradient (CG) method for electronic relaxations, accelerated using Methfessel–Paxton Fermi-level smearing with a Gaussian width of 0.2 eV [37]. The positions of the atoms are relaxed until the forces on all unconstrained atoms are less than 0.03 eV/Å. We used a $5 \times 5 \times 1$ Monkhorst–Pack mesh [38] for both $SrTiO_3$(6 2 0) and (6 2 2); this results in 9 and 13 *k*-points in the irreducible Brillouin zone, respectively. We have tested both systems with $7 \times 7 \times 1$ meshes and unbalanced *k*-point meshes and verified they have negligible impact on our results.

For bulk $SrTiO_3$ in its cubic form we obtain an optimized lattice parameter of 3.86 Å. The experimental value is 3.905 Å at room temperature [39]. Our value is of course very similar to those obtained by several other groups using DFT to examine $SrTiO_3$ [40–44]. The lattice parameter for Pt is found to be 3.92 Å using DFT–LDA versus an experimental value of 3.92 [16]. Thus, the lattice mismatch between bulk $SrTiO_3$ and Pt is predicted by DFT to be 1.5% compared to 0.4% experimentally. This small lattice mismatch is comparable to that for Pt/$BaTiO_3$ [45] and is much smaller than those of many other metal/metal oxide interfaces such as Cu/MgO [46] and Ta or W on $BaTiO_3$ [45]. In all of our calculations, the dimensions of the supercell in the plane of the surface is fixed to be a multiple of our DFT-optimized $SrTiO_3$ lattice spacing.

Our supercells for the stepped surface calculations have a slightly different configuration than was used in our earlier work on the low-Miller index surfaces. For the low-Miller index surfaces we used symmetric supercells and allowed all the atoms to relax [9,10,18]. For the stepped surfaces we adsorbed Pt on only one side of the $SrTiO_3$ surface, which allows us to use smaller slabs (see discussion below) therefore reducing the computational cost of our calculations. This geometry breaks the symmetry of the supercell in the direction normal to the surface. One consequence of this broken symmetry is that the supercell can have a net dipole in the direction normal to the surface, resulting in an spurious dipole–dipole interaction in this direction due to the use of periodic boundary conditions [47,48]. We have maintained a vacuum spacing of 15 Å in all of our calculations to minimize this dipole–dipole interaction. We have checked that applying the dipole corrections available in VASP [47] to a select set of calculations has negligible impact on the results.

In symmetric slabs the bulk behavior is recovered in the center of our slabs, but for one-sided slabs we fix a number of the bottom layers to mimic the bulk behavior. We have tested the impact of the total number of layers and the number of fixed and free layers on several test calculations for both $SrTiO_3$(6 2 0) and $SrTiO_3$(6 2 2). We define the layers in our system to be perpendicular to normal of the surface. In this definition the step edge atoms (the least coordinated atoms) on the surface compose the top layer and therefore the termination of each stepped surface is defined by the step edge atoms. Similar to the low-Miller index surfaces, stepped $SrTiO_3$ surfaces have two distinct terminations. These are discussed in more detail in Sections 3 and 4. To relate the stepped $SrTiO_3$ slabs to our low-Miller index surface calculations we note that a 14-layer slab of $SrTiO_3$(6 2 0) [$SrTiO_3$(6 2 2)] is 7.9 [7.6] Å thick, while for our seven-layer $SrTiO_3$(1 0 0) calculations we used a seven-layer slab that was 13.5 Å thick [9]. However, since our (1 0 0) slab was symmetric the effective thickness was only 5.75 Å and this is similar to the thickness used in our stepped $SrTiO_3$ calculations. This reinforces the advantage of using one-sided slabs; a symmetric slab with a similar thickness would require ∼23 layers consisting >100 atoms.

The discussion of Pt on $SrTiO_3$(6 2 0) and (6 2 2) in the subsequent sections will concentrate on the adsorption energy of Pt, E_{ads}, in various sites and the work of separation, W_{sep}. E_{ads} is defined by:

$$E_{ads} = \frac{E_{slab} + NE_{Pt,gas} - E_{ads-slab}}{N} \quad (1)$$

where E_{slab} is the total energy of the relaxed $SrTiO_3$ slab in the absence of any adsorbed Pt, $E_{Pt,gas}$ the energy of an isolated spin-polarized Pt atom, $E_{ads-slab}$ the total energy of the Pt/$SrTiO_3$ slab and N the total number of Pt atoms in the Pt/$SrTiO_3$ slab. Similarly, the work of separation is defined by [40,41,49]:

$$W_{sep} = \frac{E_{slab} + E_{Ptlayer(L)} - E_{ads-slab}}{A_{uc}} \quad (2)$$

Here, $E_{Ptlayer(L)}$ is the total energy of L layers of Pt(1 0 0) in its relaxed geometry but restricted in the plane of the layers to the lattice spacing of the $SrTiO_3$ system [36,40,41]. A_{uc} is the area of the computational supercell in the plane of the surface. As noted by Finnis [49] the work of separation defined in Eq. (2) does not exactly correspond to the value obtained experimentally due to the artificial stress placed on the Pt thin film when restricting it to the lattice parameter of $SrTiO_3$ and the neglect of other dissipative processes such as diffusion from the bulk to the freshly separated surfaces. Nevertheless, Eq. (2) provides an upper bound on the work of separation that would be observed experimentally and provides a useful measure of the strength of interaction between the metal film and metal oxide substrate [49]. We have evaluated the adsorption energy for one test site on both $SrTiO_3$(6 2 0) and (6 2 2) using 12-, 14-, and 18-layer slabs with both four and six bottom layers fixed. Using a 14-layer slab with the bottom six layers fixed for both surfaces gave adsorption energies less than 0.02 eV per atom different from the larger calculations. As a result, we used 14-layer $SrTiO_3$ slabs with six fixed layers in the remainder of our calculations.

The number of atoms in each supercell for these systems is similar to our earlier low-Miller index calculations [9,10,18]. The relaxation on these surfaces, however, is more complex than for the flat surfaces since there is less symmetry. An important practical consequence of this observation for our purposes is that calculations on the stepped surfaces are considerably more time consuming than similar calculations on flat surfaces. As will be seen in Sections 3 and 4 we must also address many more potential adsorption sites for the stepped surfaces than the low-Miller index surfaces.

3. Pt/$SrTiO_3$(6 2 0)

In this section we report our calculations to determine the favored adsorption site of Pt on stepped $SrTiO_3$(6 2 0). This surface has {1 1 0} steps and (1 0 0) terraces. As we have noted earlier the top layer on the stepped $SrTiO_3$ surfaces is defined by the step edge atoms (the lowest coordinated atoms) and the $SrTiO_3$(6 2 0) surface can be either SrTiO- or O_2-terminated. We discuss Pt adsorption at submonolayer coverages on various sites on the SrTiO- (O_2-) terminated $SrTiO_3$(6 2 0) surface in Section 3.1 (Section 3.2). We then discuss W_{sep} for Pt slabs adsorbed on both terminations of $SrTiO_3$(6 2 0) in Section 3.3.

3.1. Pt on SrTiO-terminated $SrTiO_3$(6 2 0)

Fig. 4 shows a perspective side and top view of the unit cell of the SrTiO-terminated $SrTiO_3$(6 2 0) surface along with a list of the different Pt adsorption sites we examined using DFT. Each surface unit cell has two distinct steps, which we define by the atoms composing the step edge. In this case there is a Sr and a Ti–O step. The surface also has alternating (1 0 0) oriented TiO_2 and SrO terraces. The side view in Fig. 4 shows the same unit cell in the direction perpendicular to the step edge, but multiple unit cells parallel to the step edge. There are three general types of sites for adsorption of Pt: along the bottom of the step edge, on the terrace, and finally on top of the step edge. Having two distinct steps and three types of adsorption sites yields six possible locations for the Pt atom. Since we use the smallest unit cell for this surface (indicated by the box in the top view in Fig. 4) with periodic boundary conditions, placing a Pt atom on any site will result in a row of Pt atoms along the ⟨1 0 0⟩ direction, that is, parallel to the steps. Attempting to determine the adsorption energy of an isolated Pt adatom would require much larger unit cells and is computationally prohibitive. As a result, all calculations presented below are for one Pt atom per surface unit cell. This configuration does not allow Pt atoms making up a row in the ⟨1 0 0⟩ direction to relax individually, although the Pt row can move along the ⟨1 0 0⟩ direction. To examine the impact of displacements in this direction, we tested two types of sites displaced by a half-unit cell in the ⟨1 0 0⟩ direction. Each site is identified by three pieces of information: (1) the step or terrace with which the site is associated (for SrTiO-terminated $SrTiO_3$(6 2 0) we have Sr or Ti–O steps and SrO or TiO_2 terraces) (2) the two locations along the ⟨1 0 0⟩ direction, and (3) location with respect to the step (step bottom, step edge, or terrace). The second feature has been labeled by indicating if the Pt atom would be on top of a substrate atom or in a bridge location (as seen by the top view). For example, the label edge(topSr)_Sr step denotes a Pt atom placed on the edge of the Sr step in a position where it is above a Sr atom. The edge(brg)_Sr step site is obtained by moving from the edge(topSr)_Sr step site by half a unit cell along ⟨1 0 0⟩. Similar labeling is used for the other stepped $SrTiO_3$ surfaces discussed in the rest of this paper.

Table 1 reports the adsorption energy for all the sites we examined on the SrTiO-terminated $SrTiO_3$(6 2 0) surface. We only examined one site on the terrace based on our previous $SrTiO_3$(1 0 0) calculations, which indicate Pt prefers being adsorbed on top of O atoms [9]. For both the Sr and Ti–O

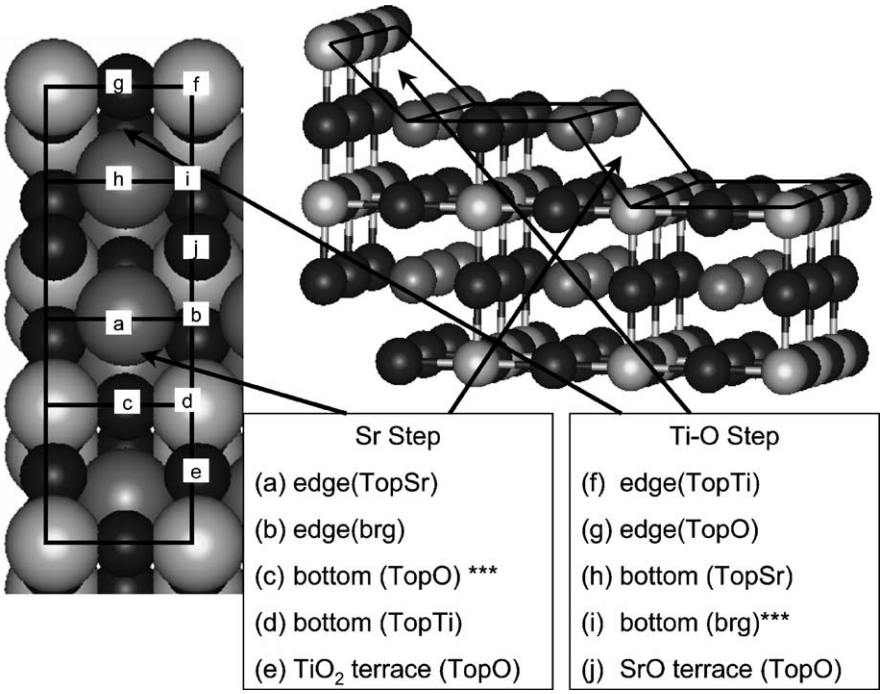

Fig. 4. Ball model of the SrTiO-terminated $SrTiO_3$(6 2 0) surface is shown in both top and perspective side view. The different adsorption sites for Pt we examined are labeled. Triple asterisks (***) indicate the most favored site based on our DFT calculations along each step. See text for more details.

step the preferred adsorption site is along the step bottoms, with an adsorption energy of ~4.35 eV per atom. When we placed Pt atoms on the terrace sites on the SrTiO-terminated $SrTiO_3$(6 2 0) surface we find that for the SrO terrace the Pt atom relaxed to the step bottom and for the TiO_2 terrace we find the adsorption energy is 3.69 eV per atom. This indicates that the Pt atom is still attracted to the step edge at these small separations. For this coverage the equivalent system for Pt on $SrTiO_3$(1 0 0) is the 1/2 ML coverage (this results in Pt atoms in every other row along the ⟨1 0 0⟩ direction). If we assume that the 1/2 ML coverage on $SrTiO_3$(1 0 0) approximates Pt adsorption on the terrace of $SrTiO_3$ surfaces vicinal to (1 0 0) we can assign a E_{ads} value of 3.77 eV per atom (3.47 eV per atom) for the SrO (TiO_2) terrace based on our earlier work [9]. Hence, when we compare the adsorption energy of our terrace sites to the favored step bottom sites we see that the step bottoms are preferred by 0.60 eV per atom (0.87 eV per atom) versus the SrO (TiO_2) terrace. This substantial energy difference indicates that we should expect to find Pt along the step edge versus the terrace on surfaces of this type. A similar result was obtained by Lodziana and Norskov [20] using DFT for Pd on stepped α-Al_2O_3(0 0 0 1) surfaces.

Table 1
E_{ads} values for the adsorption sites examined for Pt on SrTiO-terminated $SrTiO_3$(6 2 0)

Location	E_{ads} (eV per atom)
Edge(topSr)_Sr step	2.78
Edge(brg)_Sr step	4.12
Bottom(topO)_Sr step	**4.37**
Bottom(topTi)_Sr step	4.04
(TopO)_TiO_2 terrace	3.69
Edge(topTi)_Ti–O step	[a]
Edge(topO)_Ti–O step	3.81
Bottom(topSr)_Ti–O step	4.03
Bottom(brg)_Ti–O step	**4.34**
(TopO)_SrO terrace	[a]

The most favored sites along the Sr step and the Ti–O step are indicated in bold.

[a] Pt atoms placed at the sites moved to the most stable site on the Ti–O step during relaxation.

The geometry of the favored sites for Pt on both steps gives some insight into the stabilization mechanism of these sites. For the Pt adsorbed to the bottom(brg) site along the Ti–O step, Pt is bonded to the O on the SrO terrace at a distance of 2.02 Å. The Pt atom appears to gain an additional stability by electrostatic interactions with the O step edge atoms compared to Pt on top of an O atom on the flat SrO terrace. For the Pt adsorbed in bottom(topO) site along the Sr step, Pt is bonded to the Ti atom on the step bottom at a bond length of 2.74 Å.

3.2. Pt on O_2-terminated $SrTiO_3$(6 2 0)

We have performed a similar analysis to that of the previous section for Pt on O_2-terminated $SrTiO_3$(6 2 0). Fig. 5 is similar to Fig. 4 but for the O_2-terminated $SrTiO_3$(6 2 0) surface. Both steps on this surface consist of O atoms along the step edge and bottom, but they differ in the composition of the atoms in the base of the step; one step has a Sr atom

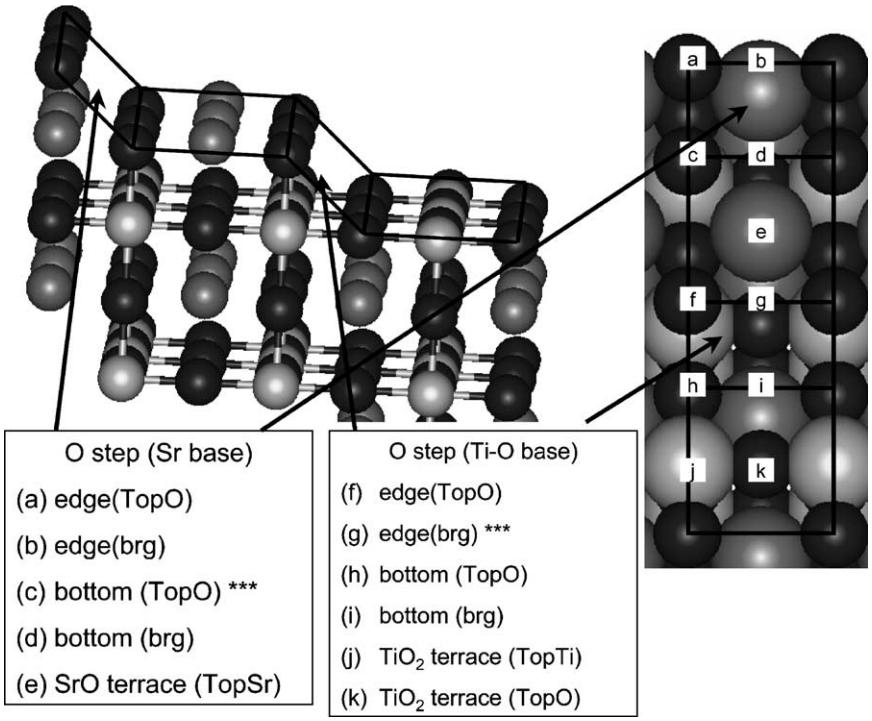

Fig. 5. Ball model of the O_2-terminated $SrTiO_3$(6 2 0) surface is shown in both top and perspective side view. The different adsorption sites for Pt we examined are labeled. Triple asterisks (***) indicate the most favored site based on our DFT calculations along each step.

base and the other a Ti–O base. To distinguish between the two steps we refer to their base in the labels.

The adsorption energy for the 11 distinct sites we examined for Pt on O_2-terminated $SrTiO_3$(6 2 0) is reported in Table 2. For the O step with the Sr base we find the strongest adsorption site is in the step bottom with a E_{ads} value of 5.36 eV per atom. This is much larger than the values we saw for the SrTiO-terminated $SrTiO_3$(6 2 0) surface. The O step with the Ti–O base has the most stable site on the bridge site on O step edge not the step bottom. One may expect that both O steps should behave similarly but we see a larger E_{ads}, by ~1.4 eV per atom, between the favored site along the O step with the Sr base compared to the O step with the Ti–O base. Pictures of the initial and final states from our DFT calculations for the two favored sites found along the step bottoms are shown in Fig. 6. The Pt atom along the O step with the Sr base undergoes an interesting relaxation where it burrows into the step, allowing it to interact with the O atom on the step edge and the step bottom (see Fig. 6(a)). The O atoms on the O step with the Ti–O base are bonded to a Ti atom. The Ti–O bond is stronger than the Sr–O bond and therefore the Pt atom cannot achieve a similar state as found on the O step with the Sr base. Despite the lower E_{ads} value on the O step with Ti–O base, this value is still larger by 0.20 eV per atom (0.50 eV per atom) than the TiO_2 (SrO) terrace. We can see from Fig. 6(b) that the Pt atom along the O step with the Ti–O base achieves strong interactions with the O atom on the step edge. The net result of these calculations is that we expect Pt to interact with the steps over the terrace for the O_2-terminated $SrTiO_3$(6 2 0) surface.

Table 2
E_{ads} for the adsorption sites examined for Pt on O_2-terminated $SrTiO_3$(6 2 0)

Location	E_{ads} (eV per atom)
Edge(topO)_O step (Ti–O base)	3.10
Edge(brg)_O step (Ti–O base)	**3.99**
Bottom(topO)_O step (Ti–O base)	3.60
Bottom(brg)_O step (Ti–O base)	3.44
(TopO)_TiO_2 terrace	3.39
(TopTi)_TiO_2 terrace	3.56
Edge(topO)_O step (Sr base)	[a]
Edge(brg)_O step (Sr base)	4.81
Bottom(topO)_O step (Sr base)	**5.36**
Bottom(brg)_O step (Sr base)	4.57
(TopO)_SrO terrace	[a]

The most favored sites along both steps are indicated in bold.
[a] Pt atoms placed initially at the sites moved to other sites during relaxation.

3.3. W_{sep} for Pt/$SrTiO_3$(6 2 0)

We have also calculated W_{sep} of Pt slabs on the $SrTiO_3$(6 2 0) surface to determine the interface strength. In our earlier work of Pt on the low-Miller index $SrTiO_3$ surfaces, we found that a larger W_{sep} correlates well with the likelihood (or the ease) of observing epitaxial growth experimentally [11]. To evaluate W_{sep} we adsorbed three- and nine-layer thick Pt(6 2 0) slabs on both terminations of

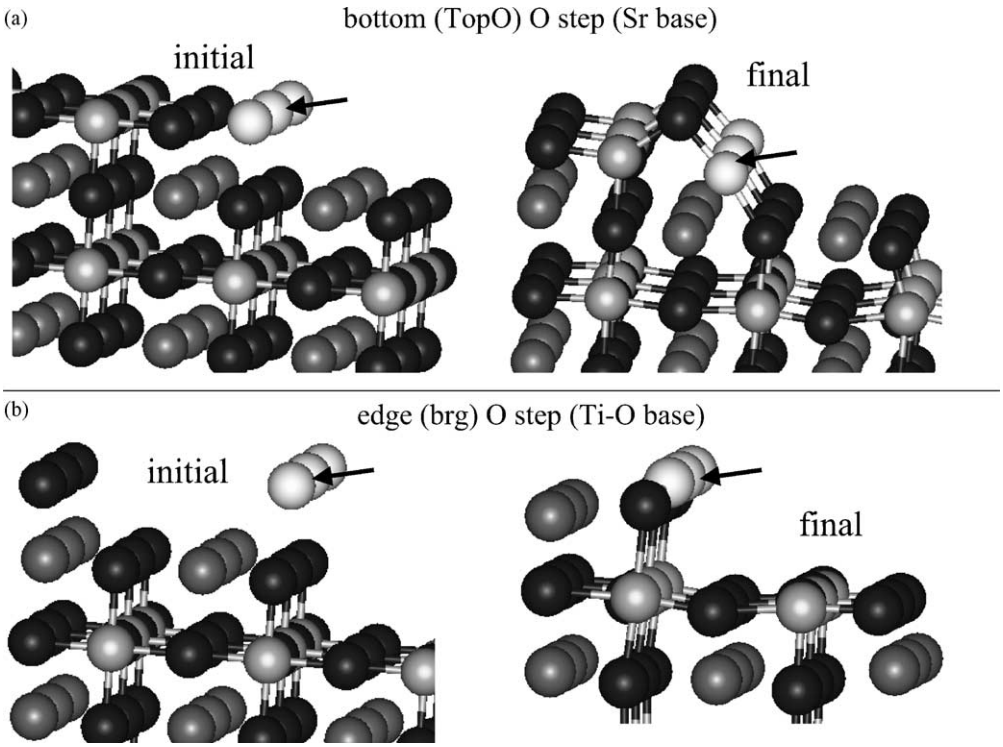

Fig. 6. Ball model illustrating the initial and final state from our DFT calculation of Pt on the most favored site along the O step (a) with Sr base and (b) with Ti–O base for the O_2-terminated $SrTiO_3$(6 2 0) surface. The Pt atoms are represented by white balls and also marked by an arrow to assist the reader. The key for the other atoms remains the same as in Fig. 2.

$SrTiO_3$(6 2 0). A Pt layer is defined normal to the (6 2 0) surface and therefore there are two Pt atoms per layer. Ideally we would like to vary the Pt slab thickness until W_{sep} has converged to a value independent of the film thickness, but this creates more computationally demanding calculations. A nine-layer Pt(6 2 0) slab is slightly thicker than a three-layer Pt(1 0 0) slab and we found in our earlier study of Pt on $SrTiO_3$(1 0 0) that W_{sep} converges by this thickness [9], so we anticipate that our nine-layer slab is sufficiently thick to recover the thick film limit. The three-layer Pt(6 2 0) slab is similar in thickness to a single monolayer on Pt(1 0 0). Since we are covering the entire surface with Pt we need only perform two sets of calculations for each termination. In the first configuration, denoted as fcc, the Pt atoms are placed in the fcc sites defined by treating the Sr and O atoms as Pt atoms. The second configuration, denoted as top, is obtained by displacing the Pt atoms by a half-unit cell in the ⟨1 0 0⟩ direction. The fcc configuration would be favored for a Pt slab adsorbed on a Pt(6 2 0) surface.

The E_{ads} and W_{sep} values are reported for Pt(6 2 0) slabs on both terminations of $SrTiO_3$(6 2 0) in Table 3. Comparing the E_{ads} values in Tables 2 and 3 shows that the adsorption energy for Pt increases going from rows of Pt atoms to the Pt slabs. That is, Pt atoms on the surface gain stability from Pt to Pt interactions. Examining the W_{sep} values for the SrTiO-termination, we observe a reversal of the favored configuration in going from a three-layer, where the top configuration is favored, to nine-layer Pt(6 2 0) slab, where the fcc configuration becomes favored by 0.18 J/m^2. This implies that kinetics of the system may have an impact on the actual observed configurations for this termination. For the O_2-termination the top configuration is favored for both terminations in both the three- and nine-layer slab. W_{sep} drops as the slab thickness is changed from three to nine layers for O_2-termination, indicating that the interface strength weakens slightly due to the increased Pt–Pt interactions. We find a W_{sep} value of 4.79 J/m^2 (4.66 J/m^2) for a nine-layer Pt slab on the SrTiO- (O_2-) terminated surface. The W_{sep}

Table 3
E_{ads} and W_{sep} values for a three-layer and nine-layer thick Pt(6 2 0) slab adsorbed on SrTiO3(6 2 0) in the fcc and top configuration

Configuration	E_{ads} (eV per atom)	W_{sep} (J/m^2)
SrTiO-terminated $SrTiO_3$(6 2 0)		
Three-layer fcc	5.59	4.63
Three-layer top	5.68	5.20
Nine-layer fcc	6.48	4.79
Nine-layer top	6.46	4.51
O_2-terminated $SrTiO_3$(6 2 0)		
Three-layer fcc	5.49	4.46
Three-layer top	5.57	4.91
Nine-layer fcc	6.36	3.45
Nine-layer top	6.43	4.66

As described in the text, the nine-layer fcc configuration on the SrTiO-terminated surface was not converged to the same level as the other results.

for Pt/$SrTiO_3$(1 0 0) is less than 2 J/m^2, indicating that the Pt/$SrTiO_3$(6 2 0) interface is considerably stronger. We also evaluated W_{sep} for a nine-layer Pt(6 2 0) slab being separated from a 14-layer Pt(6 2 0) slab in the same restricted lattice spacing of 3.86 Å, and found a value of 13.1 J/m^2. This shows that the Pt–$SrTiO_3$ interface for the (6 2 0) system is still much weaker than the Pt–Pt interactions.

It is useful to connect the results from our Pt slab calculations with the single Pt atom calculations of Sections 3.1 and 3.2. For the O_2-terminated surface we found that the most favored Pt adsorption site was on top of the O atom in O step bottoms. The top configuration for the Pt slab allows the Pt atom at the step bottom to be at the most favored site, reinforcing the expectation that the top configuration should be observed for Pt films deposited on the O_2-terminated $SrTiO_3$(6 2 0) surface. For the SrTiO-terminated surface, a bridge site was preferred for Pt rows adjacent to the Ti–O step but for the Sr step Pt atom prefers to sit on top of the O atom, with the latter site having a considerably larger E_{ads} than the former. For Pt slabs, the top configuration allows the Pt atoms to be in the favored site along the Sr step but not along the Ti–O step. The reverse is true for the fcc configuration, which allows the Pt atom to be in the favored site along the Ti–O step. The energy differences between the favored site along the Sr and Ti–O step are negligible (<0.03 eV per atom) and as noted earlier there is a reversal of the favored configuration based on W_{sep} from the fcc configuration favored for the three-layer to the top configuration for the nine-layer slab. This reinforces the expectation that one may see a mixture of both configurations on the SrTiO-termination and that kinetics may determine the observed configuration.

4. Pt/$SrTiO_3$(6 2 2)

In this section we report on our calculations for Pt on the $SrTiO_3$(6 2 2) surface. This surface has (1 0 0) terraces and {1 1 1} steps. Two surface terminations are possible, as defined by the step edge atoms, a SrO_3-termination and a Ti-termination. The Ti-termination is very similar to the SrO_3-termination except for the appearance of an additional Ti atom on one of the step bottoms (compare Figs. 7 and 8). The $SrTiO_3$(6 2 2) surfaces have narrower terraces than the $SrTiO_3$(6 2 0). One result of this difference is that to adsorb a row of Pt atoms along the step edge for the (6 2 2) surface we must use two Pt atoms per supercell. This configuration allows relaxation of individual Pt atoms in the ⟨1 1 0⟩ direction. As a result, we generally see much stronger relaxation for this system than for $SrTiO_3$(6 2 0). The $SrTiO_3$(6 2 2) surface has two types of steps for each termination, but there are only two types of sites on these surfaces, step edge and bottom. We could have studied a stepped $SrTiO_3$ surface with larger terraces but this makes the unit cell substantially larger. This may be worth examining in the future (see Section 5). The adsorption energies in this section cannot be compared to the 1/2 ML results for the $SrTiO_3$(1 0 0) as we did for $SrTiO_3$(6 2 0) since the Pt atoms are not organized into rows in the ⟨1 0 0⟩ direction. The appropriate comparison for $SrTiO_3$(6 2 2) is Pt adsorbed along the ⟨1 1 0⟩ direction of a (2 × 2) $SrTiO_3$(1 0 0) cell at 1/2 ML coverage. We have performed these calculations on the (2 × 2) $SrTiO_3$(1 0 0) cell using the same parameters as in our earlier work on Pt/$SrTiO_3$(1 0 0) (see [9] for details) for both the SrO- and TiO_2-termination. We found E_{ads} is 4.06 eV per atom (4.45 eV per atom) for the SrO- (TiO_2-) termination

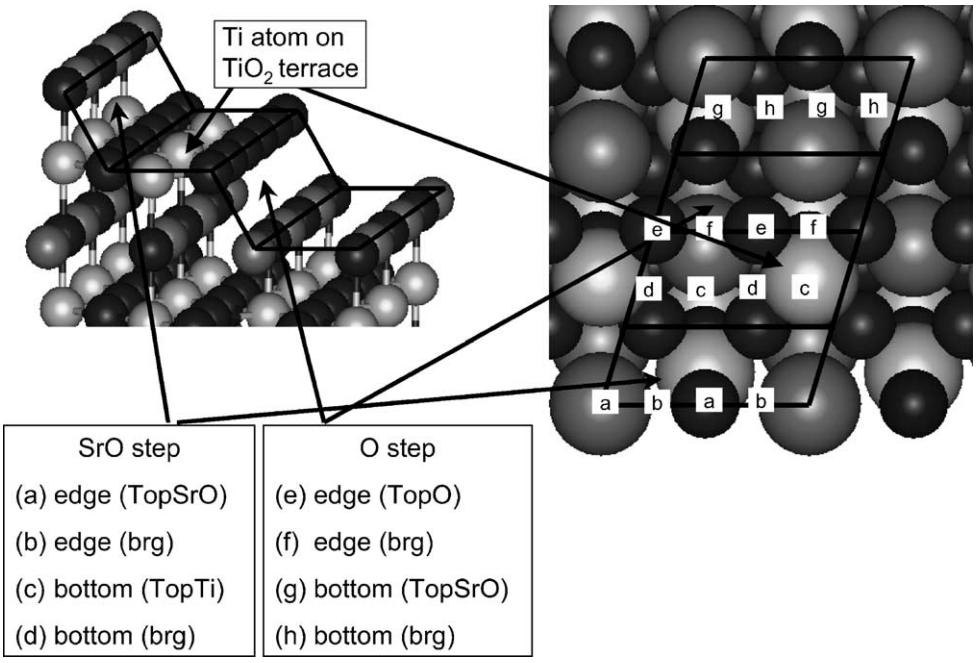

Fig. 7. Ball model of the SrO_3-terminated $SrTiO_3$(6 2 2) surface is shown in both top and perspective side view. The different adsorption sites for Pt we examined are labeled.

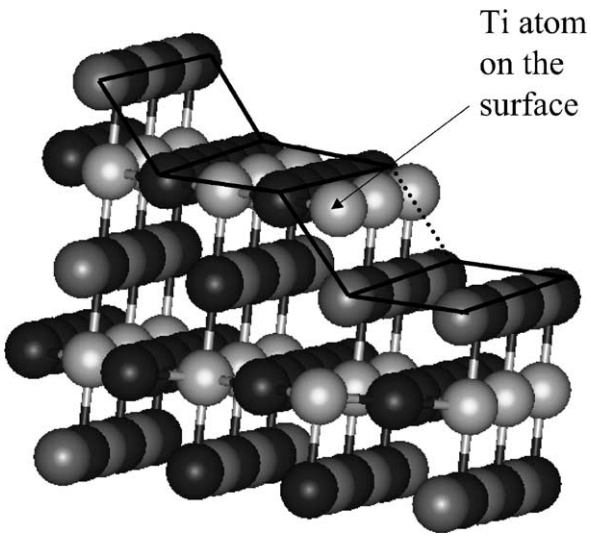

Fig. 8. Ball model of the Ti-terminated $SrTiO_3$(6 2 2) surface.

where the Pt atom sits on the Sr and O atoms (O atoms) along the ⟨1 1 0⟩ direction. We discuss Pt adsorption on various sites on SrO_3- (Ti-) terminated $SrTiO_3$(6 2 2) in Section 4.1 (Section 4.2) and W_{sep} for Pt slabs on $SrTiO_3$(6 2 2) in Section 4.3.

4.1. Pt on SrO_3-terminated $SrTiO_3$(6 2 2)

Fig. 7 shows a perspective side and top view of the unit cell of SrO_3-terminated $SrTiO_3$(6 2 2) along with a list of the Pt adsorption sites we examined. This surface consists of alternating SrO and O steps with TiO_2 and SrO terraces below. The Pt atoms do not adsorb directly on top of substrate atoms for the (6 2 2) surface, but we have labeled Pt atoms as being on top of a substrate atom if it interacts closely with an atom on the surface. The adsorption energies associated with the eight sites we have considered are summarized in Table 4. Table 4 indicates that the bottom step edges are favored at values of 5.78 and 5.33 eV per atom. As noted above, for 1/2 ML Pt adsorbed along the ⟨1 1 0⟩ direction on $SrTiO_3$(1 0 0) we found an adsorption energy of 4.06 eV per atom (4.45 eV per atom) for the SrO (TiO_2) terrace. This indicates, that similar to $SrTiO_3$(6 2 0), Pt adsorption on the step edges of $SrTiO_3$(6 2 2) is preferred relative to adsorption on $SrTiO_3$(1 0 0) terraces by around 1 eV.

Table 4
E_{ads} for the adsorption sites examined for Pt on SrO_3-terminated $SrTiO_3$(6 2 2)

Location	E_{ads} (eV per atom)
Edge(topSrO)_SrO step	4.74
Edge(brg)_SrO step	4.57
Bottom(topTi)_SrO step	**5.33**
Bottom(brg)_SrO step	5.28
Edge(topO)_O step	5.33
Edge(brg)_O step	5.50
Bottom (topSrO)_O step	**5.78**
Bottom(brg)_O step	5.22

The most favored sites along both steps are indicated in bold.

One complication in describing Pt adsorption on $SrTiO_3$(6 2 2) is that for many of the adsorption sites there was a dramatic rearrangement of both the Pt atoms and the substrate atoms during relaxation to the final adsorption site. This is illustrated in Fig. 9, which shows the initial and final state of Pt adsorbed in the most favored site found on SrO_3-terminated $SrTiO_3$(6 2 2). Comparing Figs. 6, 7 and 9 show that the $SrTiO_3$(6 2 2) surface may undergo more substantial reconstruction of the step edge due to the presence of Pt than $SrTiO_3$(6 2 0). It is not clear from these preliminary results how this would affect subsequent Pt atom incorporation or the step structure. Furthermore, the Pt atom in this site interacts with both the O and SrO steps due to the narrow terrace of this surface. In stepped structures with wider terraces these type of interactions cannot occur. A more detailed study with wider terraces would be needed to clarify the general behavior of Pt on the SrO_3-terminated stepped $SrTiO_3$ surfaces with (1 0 0) terraces.

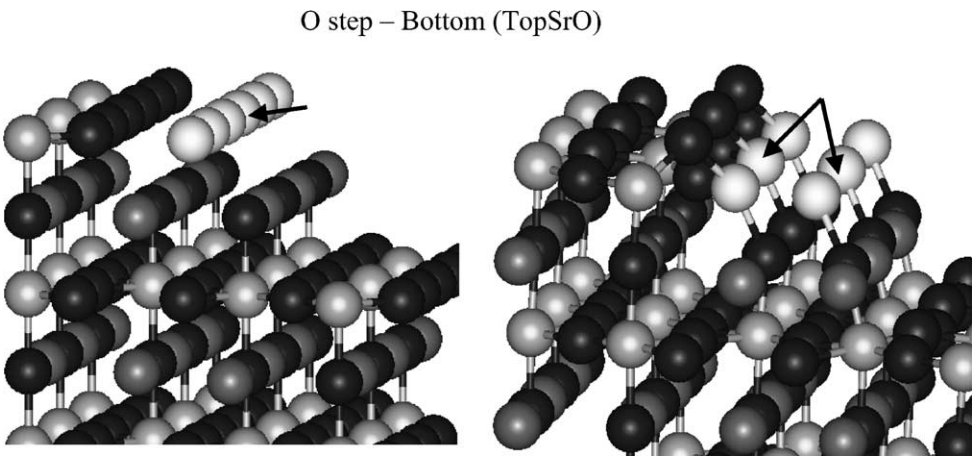

Fig. 9. Ball model illustrating the initial and final state from our DFT calculation of Pt on the most favored site along the O step for the SrO_3-terminated $SrTiO_3$(6 2 2) surface. Arrows indicate the Pt atoms.

Table 5
E_{ads} values for the various adsorption sites examined for Pt on Ti-terminated $SrTiO_3$(6 2 2)

Location	E_{ads} (eV per atom)
Edge(topSrO)_SrO step	[a]
Edge(brg)_SrO step	[a]
Bottom(topTi)_SrO step	4.87
Bottom(brg)_SrO step	5.11
Edge(topO)_O step	[a]
Edge(brg)_O step	5.29
Bottom(topSrO)_O step	**5.82**
Bottom(brg)_O step	**5.79**

The most favored sites along both steps are indicated in bold.
[a] Pt atoms placed initially at the sites moved to one of the most favored sites during relaxation.

4.2. Pt on Ti-terminated $SrTiO_3$(6 2 2)

For Ti-terminated $SrTiO_3$(6 2 2) we examined the same sites as for the SrO_3-termination because the only difference between these surfaces is the addition of a Ti atom on the step bottom associated with the O step edge. This can be seen in Fig. 8, which shows a perspective side of Ti-terminated $SrTiO_3$(6 2 2). To define the possible adsorption sites on this surface, we used the same initial states as the SrO_3-terminated surface, ignoring the presence of the Ti atom, and allowed the relaxation to incorporate the effects of the Ti atom.

The results of our calculations are summarized in Table 5. Many of the sites relaxed to the bottom of the O step where the additional surface Ti atom is located. As might be expected, the addition of the Ti atom greatly impacts the sites on both the O step and SrO step. We find for the favored sites indicated in bold in Table 5 that the Pt incorporates itself into the step by distorting the O atoms in the adjacent SrO step (see Fig. 10). This configuration is reached by many of the initial adsorption sites we examined. Examining Fig. 10, we could conclude that we have a new type of step since the SrO step has been converted to an step with Pt–O microfacet. While these structures are interesting it is difficult to predict their impact on possible step-flow growth. We would also expect that step structures with wider terraces would not undergo such behavior since the Pt atom attached to the O step could not interact with the SrO step. The behavior of Pt on these steps cannot be simply extended out to the general class of stepped $SrTiO_3$ surfaces with {1 1 1} steps and (1 0 0) terraces without examining surfaces with wider terraces.

4.3. W_{sep} for Pt/$SrTiO_3$(6 2 2)

As we did for Pt/$SrTiO_3$(6 2 0) we determined W_{sep} for Pt(6 2 2) slabs adsorbed on both terminations of $SrTiO_3$(6 2 2). A single layer of Pt on the (6 2 2) unit cell consists of four atoms versus two atoms for the (6 2 0) surface. Because of this we evaluated W_{sep} at two layers (eight Pt atoms) and five layers (20 Pt atoms) and as before this was done for the fcc and top configuration. Unlike the pronounced relaxations that we found for rows of Pt adatoms placed on $SrTiO_3$(6 2 2), the W_{sep} calculations are well behaved and the Pt(6 2 2) slab retains its basic structure. Our results are summarized in Table 6. Similar to Pt/$SrTiO_3$(6 2 0) the top configuration is favored over the fcc configuration for both terminations of $SrTiO_3$(6 2 2). This is consistent with the fact that while the Pt adatom calculations described in Sections 4.1 and 4.2 underwent substantial relaxation, the favored sites all match the top configuration. With five layers of Pt, we find a W_{sep} value of 7.29 J/m^2 (6.91 J/m^2) for SrO_3- (Ti-) terminated $SrTiO_3$(6 2 2). These values are substantially larger than on any of the low index planes of $SrTiO_3$ [9–11] or on $SrTiO_3$(6 2 0) system (see above). This suggests, if we use W_{sep} as the only evaluation

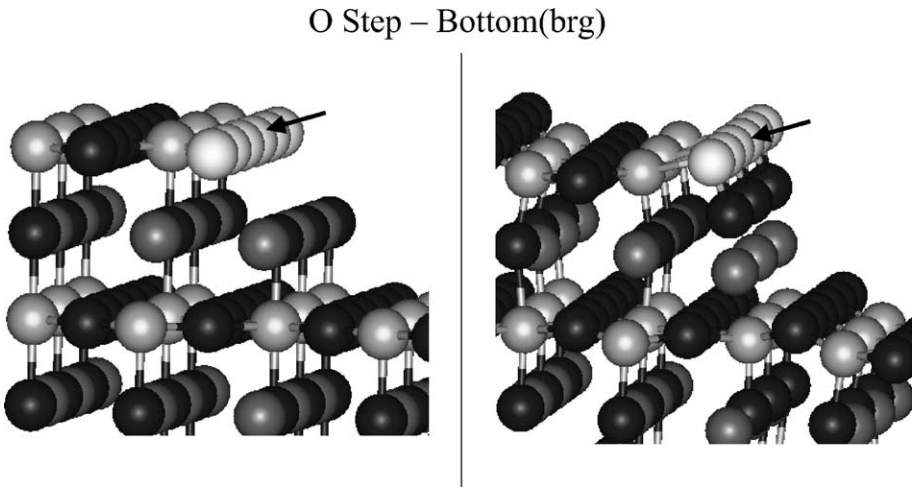

Fig. 10. Ball model illustrating the initial and final state from our DFT calculation of Pt on the O step-bottom(brg) site, one of the most favored site along the O step for Ti-terminated $SrTiO_3$(6 2 2). Arrows indicate the Pt atoms.

Table 6
E_{ads} and W_{sep} values for two-layer and five-layer thick Pt(6 2 2) slabs adsorbed on $SrTiO_3$(6 2 2) in the fcc and top configuration

Configuration	E_{ads} (eV per atom)	W_{sep} (J/m^2)
SrO_3-terminated $SrTiO_3$(6 2 0)		
Two-layer fcc	6.05	3.70
Two-layer top	6.18	4.59
Five-layer fcc	6.53	4.99
Five-layer top	6.66	7.29
Ti-terminated $SrTiO_3$(6 2 2)		
Two-layer fcc	6.15	4.37
Two-layer top	6.22	4.83
Five-layer fcc	6.54	5.24
Five-layer top	6.64	6.91

parameter, that Pt will grow epitaxially with greater ease on $SrTiO_3$(6 2 2) than on any of the other $SrTiO_3$ surfaces we have examined. It would be interesting to evaluate this conjecture experimentally.

5. Conclusion and future work

The long term aim of this work has been to suggest paths that may lead to practical means of achieving epitaxial growth of chiral metal surfaces on chiral metal oxide substrates. We conclude by summarizing our conclusions based on our work on Pt adsorption on low-Miller index $SrTiO_3$ surfaces and the stepped $SrTiO_3$ surfaces vicinal to (1 0 0). We have argued based on our results on the low-Miller index $SrTiO_3$ surfaces that among all of the possible stepped $SrTiO_3$ surfaces, those vicinal to (1 0 0) may be the best candidates for step-flow growth of deposited Pt films. We have evaluated the energetics of Pt adsorption on two achiral stepped $SrTiO_3$ surfaces vicinal to (1 0 0), $SrTiO_3$(6 2 0) and $SrTiO_3$(6 2 2). In both cases, the adsorption energy of Pt is larger along the step edges than on (1 0 0) terraces and we expect that this should strongly promote step-flow growth in these systems. Moreover, we found that the work of separation for Pt films on these stepped surfaces is substantially larger than on any of the low-Miller index surfaces of $SrTiO_3$. Since our earlier work has shown that larger values of W_{sep} correlate well with ease of achieving epitaxial growth, these results provide a strong indication that stepped $SrTiO_3$ surfaces vicinal to (1 0 0) will provide good substrates for epitaxial growth of stepped Pt films.

The step structures on $SrTiO_3$(6 2 0) prefer Pt adsorption along the step bottoms and the substrate does not undergo dramatic relaxation. The behavior found for Pt on $SrTiO_3$(6 2 0) is expected to be similar to the general class of stepped $SrTiO_3$ surfaces vicinal to (1 0 0) with {1 1 0} steps. For the $SrTiO_3$(6 2 2) surfaces we found dramatic relaxation for both terminations upon adsorption of Pt. The impact of this relaxation on the growth properties of Pt is not clear. Furthermore, we observed strong Pt interactions with both steps due to narrow terrace on $SrTiO_3$(6 2 2). This behavior cannot be easily correlated to behavior of Pt on stepped $SrTiO_3$ surfaces having {1 1 1} steps separated by wider (1 0 0) terraces. One avenue of future work that could be pursued is a more thorough investigation of the impact of step–step separation. Such a study could be very time consuming due to the combination of computationally demanding calculations with a large number of surface configurations that must be examined. It is not clear to us if calculations of this type are the most efficient approach to gain further insight into the question of which substrate is the best candidate for growth of chiral Pt films.

An alternative approach maybe to abandon the study of different Pt adsorption sites in favor of examining thicker Pt slabs on various stepped and chiral $SrTiO_3$ surfaces to evaluate the interface strength by calculating W_{sep}. Relaxation in these systems is less pronounced because Pt will be restricted by symmetry. There are also many fewer configurations to examine for a particular surface. This approach may allow us to map the interface strength as a function of the identity of the steps and terraces and in doing so study the affect of terrace width. Attempting to corroborate W_{sep} with experimentally evaluations of the Pt films on the same $SrTiO_3$ surface as the DFT calculations would be useful in evaluating the value of this approach.

Interestingly, recent experiments by Francis and Salvador depositing Pt on chiral $SrTiO_3$(6 2 1) substrates (see Fig. 3(c) for a representation of this surface) have shown that Pt films with a net (6 2 1) orientation can be obtained [50]. As shown in Fig. 3, the step edges on $SrTiO_3$(6 2 1) are combinations of the step edges in the two achiral surfaces we have studied in this paper. Our calculations and the experiments of Francis and Salvador strongly suggest that the small terraces on these surfaces promote step-flow growth of Pt, thus providing a means to increase the surface areas that can be achieved for chiral metal surfaces.

Acknowledgements

We gratefully acknowledge many useful conversations with P. Salvador, L. Porter, A. Francis, and A. Gellman and a grant of computer time at the Pittsburgh Supercomputer Center. DSS is an Alfred P. Sloan fellow and a Camille Dreyfus Teacher-Scholar. This work was supported by the NSF Grant No. CTS-0216170.

References

[1] D.S. Sholl, A. Asthagiri, T.D. Power, J. Phys. Chem. B 105 (2001) 4771.
[2] G.A. Attard, J. Phys. Chem. B 105 (2001) 3158.
[3] J.D. Horvath, A.J. Gellman, J. Am. Chem. Soc. 123 (2001) 7953.
[4] R.M. Hazen, D.S. Sholl, Nat. Mater. 2 (2003) 367.
[5] C.F. McFadden, P.S. Cremer, A.J. Gellman, Langmuir 12 (1996) 2483.
[6] D.S. Sholl, Langmuir 14 (1998) 862.

[7] K.B. Lipkowitz, et al., J. Org. Chem. 63 (1998) 732.
[8] P.S. Halasyamani, K.R. Poeppelmeier, Chem. Mater. 10 (1998) 2753.
[9] A. Asthagiri, D.S. Sholl, J. Chem. Phys. 116 (2002) 9914.
[10] A. Asthagiri, et al., Surf. Sci. 537 (2003) 134.
[11] A. Asthagiri, A.J. Francis, P. Salvador, L. Porter, D.S. Sholl, in preparation.
[12] B. Meyer, J. Padilla, D. Vanderbilt, Faraday Discuss. 114 (1999) 395.
[13] T. Yoshimura, N. Fujimura, T. Ito, J. Cryst. Growth 174 (1997) 790.
[14] P.J. Moller, S.A. Komolov, E.F. Lazneva, Surf. Sci. 425 (1999) 15.
[15] T. Wagner, et al., Zeitschrift Fur Metallkunde 92 (2001) 701.
[16] A.D. Polli, et al., Surf. Sci. 448 (2000) 279.
[17] C. Noguera, J. Phys. Condens. Mat. 12 (2000) R367.
[18] A. Asthagiri, D.S. Sholl, in preparation.
[19] Z.Y. Zhang, M.G. Lagally, Science 276 (1997) 377.
[20] Z. Lodziana, J.K. Norskov, Surf. Sci. 518 (2002) L577.
[21] K.H. Hansen, et al., Phys. Rev. Lett. 83 (1999) 4140.
[22] N. Erdman, et al., Nature 419 (2002) 55.
[23] X.G. Wang, A. Chaka, M. Scheffler, Phys. Rev. Lett. 84 (2000) 3650.
[24] O. Dulub, U. Diebold, G. Kresse, Phys. Rev. Lett. 90 (2003) 16102.
[25] K. Reuter, M. Scheffler, Phys. Rev. B 65 (2001) 35406.
[26] G. Kresse, J. Furthmuller, Comput. Mater. Sci. 6 (1996) 15.
[27] G. Kresse, J. Furthmuller, Phys. Rev. B 54 (1996) 11169.
[28] G. Kresse, J. Hafner, Phys. Rev. B 49 (1994) 14251.
[29] G. Kresse, J. Hafner, Phys. Rev. B 47 (1993) 558.
[30] A. Pasquarello, et al., Phys. Rev. Lett. 69 (1992) 1982.
[31] K. Laasonenx, et al., Phys. Rev. B 55 (1993) 13953.
[32] D. Vanderbilt, Phys. Rev. B 41 (1990) 7892.
[33] G. Kresse, J. Hafner, J. Phys. Condens. Mat. 6 (1994) 8245.
[34] D.M. Ceperley, B.J. Alder, Phys. Rev. Lett. 45 (1980) 566.
[35] A. Bogicevic, D.R. Jennison, Phys. Rev. Lett. 82 (1999) 4050.
[36] A. Christensen, E.A. Carter, J. Chem. Phys. 114 (2001) 5816.
[37] M. Methfessel, A.T. Paxton, Phys. Rev. B 40 (1989) 3616.
[38] H.J. Monkhorst, J.D. Pack, Phys. Rev. B 13 (1976) 5188.
[39] A. Pojani, F. Finocchi, C. Noguera, Surf. Sci. 442 (1999) 179–198.
[40] T. Ochs, S. Kostlmeier, C. Elsasser, Integr. Ferroelectr. 32 (2001) 959.
[41] T. Ochs, C. Elsasser, Zeitschrift Fur Metallkunde 93 (2002) 406.
[42] J. Padilla, D. Vanderbilt, Surf. Sci. 418 (1998) 64.
[43] S. Kimura, et al., Phys. Rev. B 51 (1995) 11049.
[44] Z.Q. Li, et al., Phys. Rev. B 58 (1998) 8075.
[45] F.Y. Rao, et al., Phys. Rev. B 55 (1997) 13953.
[46] R. Benedek, Phys. Rev. Lett. 84 (2000) 3362.
[47] L. Bengtsson, Phys. Rev. B. 59 (1999) 12301.
[48] J.M. Carlsson, Comput. Mater. Sci. 22 (2001) 24.
[49] M.W. Finnis, J. Phys. Condens. Mat. 8 (1996) 5811.
[50] A. Francis, P.A. Salvador, Private communication.